Miller Range 090036

Anorthositic regolith breccia

244.83 g

Figure 1: *MIL 090036 as recovered in the field. Field photo image(s) courtesy of the* ***ANSMET*** *Program, Case Western Reserve Univ. and the Univ. of Utah.*

Introduction: The 2009-10 season ANSMET team recovered MIL 090036 which was classified as a lunar anorthositic breccia (**Figure 1**) and reported in the Antarctic Meteorite Newsletter 33 no. 2 (Satterwhite and Righter, 2010). MIL 090036 was found in the middle Icefield area of the Miller Range (**Figure 2**), near MIL 07006 and MIL 090034. Cosmic ray exposure age data for MIL 090036 indicates it is not paired with any other MIL lunar meteorites (Nishiizumi and Caffee, 2013), even these two that were recovered close by.

Petrography and Mineralogy: MIL 090036 is a feldspathic polymict regolith breccia with a fine-grained to glassy matrix, and clasts that range from <0.1 mm to 2 mm in size. The clasts are dominated by monomict plagioclase grains and impact-melt breccias, with smaller amounts of granulitic breccias with olivine or ilmenite. Some clast bearing impact-melt breccia clasts have the largest sizes (up to 3 mm). All the clasts are embedded in a fine-grained to glassy matrix, which is dark colored in hand specimen (Calzada-Diaz et al., 2016) (**Figures 3, 4, and 5**).

The diversity of clasts is documented in two studies – Xie et al. (2014) studied section ,26 and Calazada-Diaz et al. (2016) studied section ,34 (**Figure 6 and 7**). Calzada-Diaz et al. (2016) found a wide variety of lithologies including granulitic breccias, impact melt breccias, and anorthositic clasts (**Figure 8**). Similarly, Xie et al. (2014) found a wide variety of lithologies including granulitic breccias, impact melt breccias, as well as plagioclase and pyroxene mineral clasts and fragments (**Figure 9**). Glassy matrix is reported in most studies (i.e., Liu et al., 2011, Xie et al., 2014, Calzada-Diaz et al., 2016).

Pyroxene and olivine Fe/Mn ratios fall as expected along a line defined by lunar samples, distinct from terrestrial or martian olivine and pyroxene (**Fig. 10**). Pyroxenes in clasts and mineral fragments from MIL 090036 exhibit a wide range of compositions from En_{90} to En_{20} (**Figures 11-14**). Plagioclase feldspar is more sodic than the other MIL 09 lunar breccias, but it is nonetheless An_{80-90}. Olivines in the MIL 090036 clasts and fragments are forsteritic in general with a range from Fo_{80} to Fo_{90}. The combination of feldspar and pyroxene compositions demonstrate the distinctly more sodic compositions and the shift away from ferroan anorthosites (FANs) and the other MIL 09 breccias (**Fig. 12-13**).

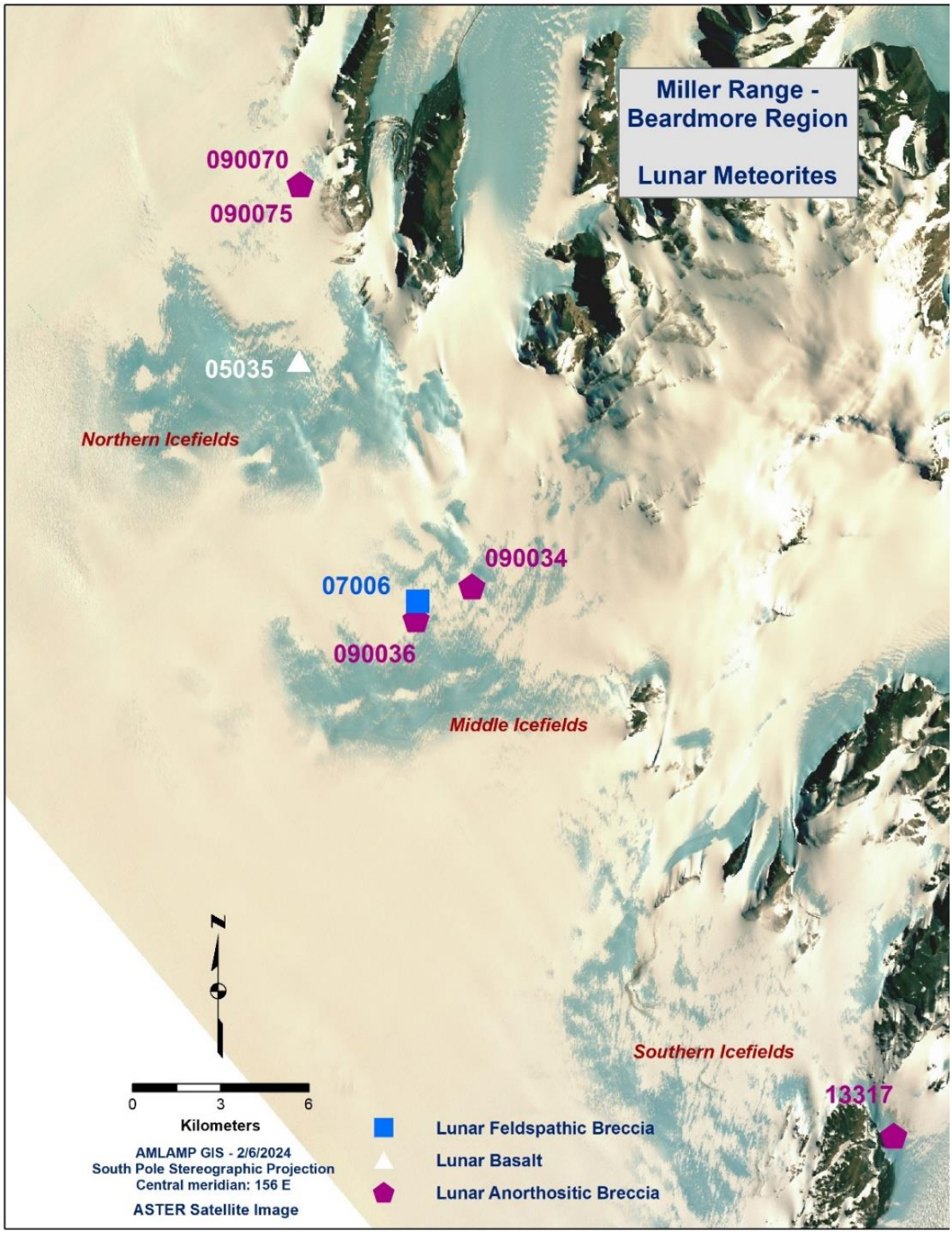

Figure 2: *Location of MIL 090036 lunar meteorite from the Miller Range 2009-10 ANSMET season, in the middle icefield of the Miller Range (purple pentagon).*

Figure 3: *Orthogonal views of lunar meteorite MIL 090036, illustrating the yellowish-brown fusion crust, and brecciated interior including many clearly feldspathic (white) clasts and mineral fragments.*

Figure 4: *Interior photo of MIL 090036, illustrating the brecciated texture and the light colored clasts in a dark matrix.*

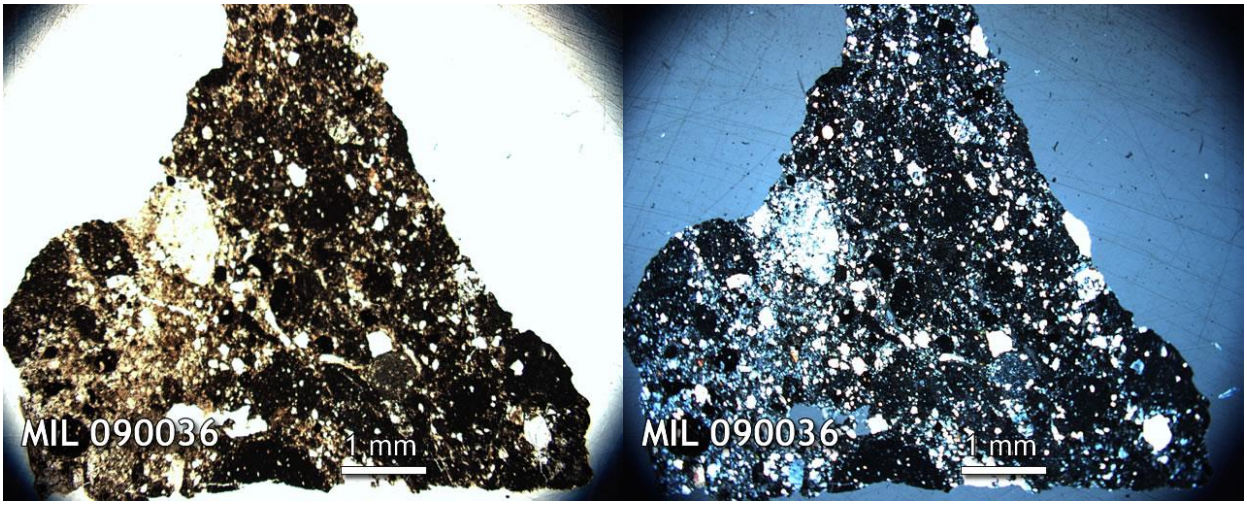

Figure 5: *Microscopic images of MIL 090036, illustrating the brecciated texture. Plane polarized (left) and cross polarized (right) light images of the library section.*

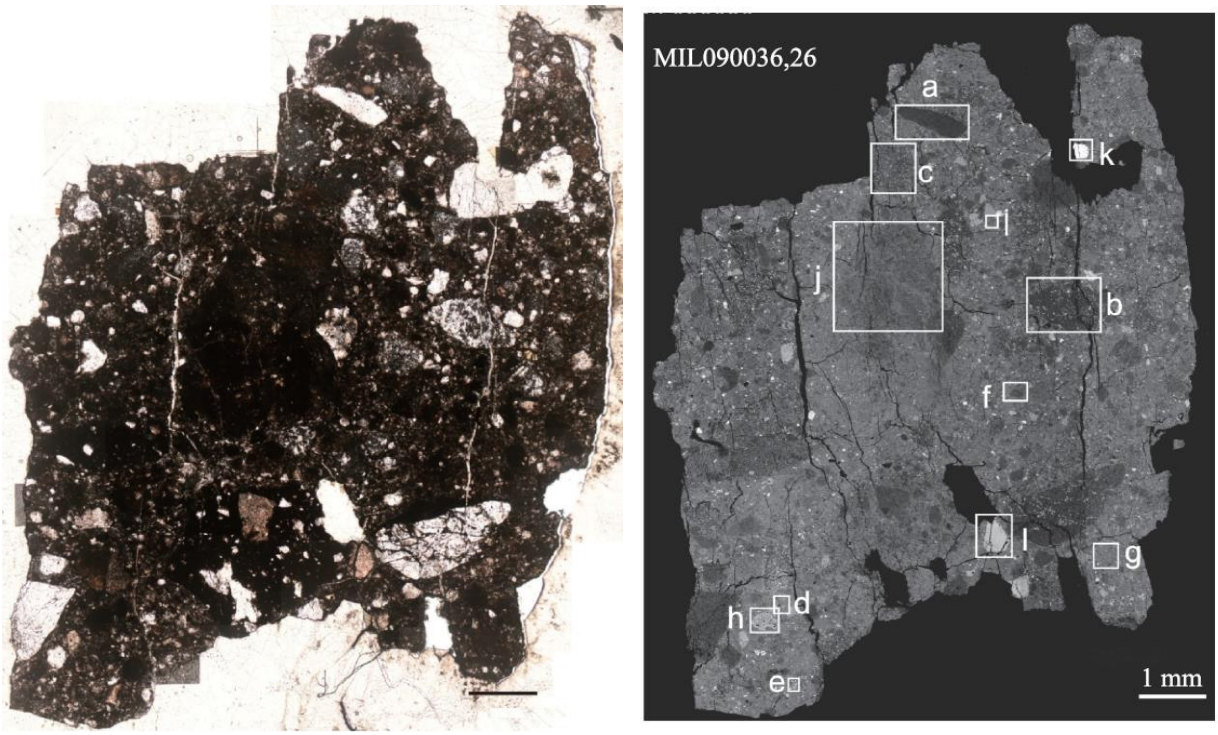

Figure 6: *plane polarized light image of MIL 090036 ,26 (left) and BSE image of MIL 090036 ,26 (right). Clasts labelled in (b) are shown in detail in Figure 9 (figures from Xie et al., 2014).*

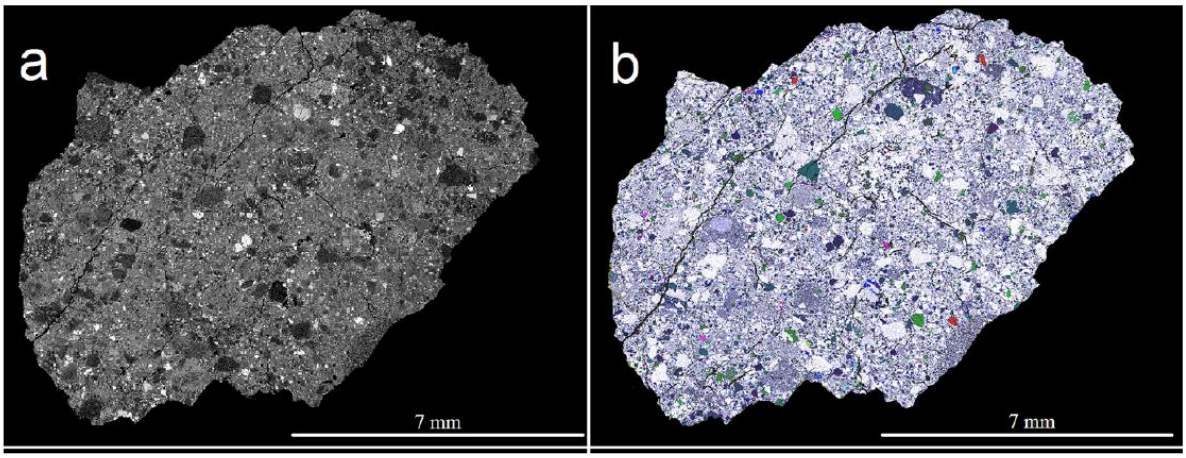

Figure 7: *(a) BSE image of MIL 090036, 34; (b) False-color element map of MIL 090036, 34 showing distribution and qualitative concentration of elements present (from Calzada-Diaz et al. 2016).*

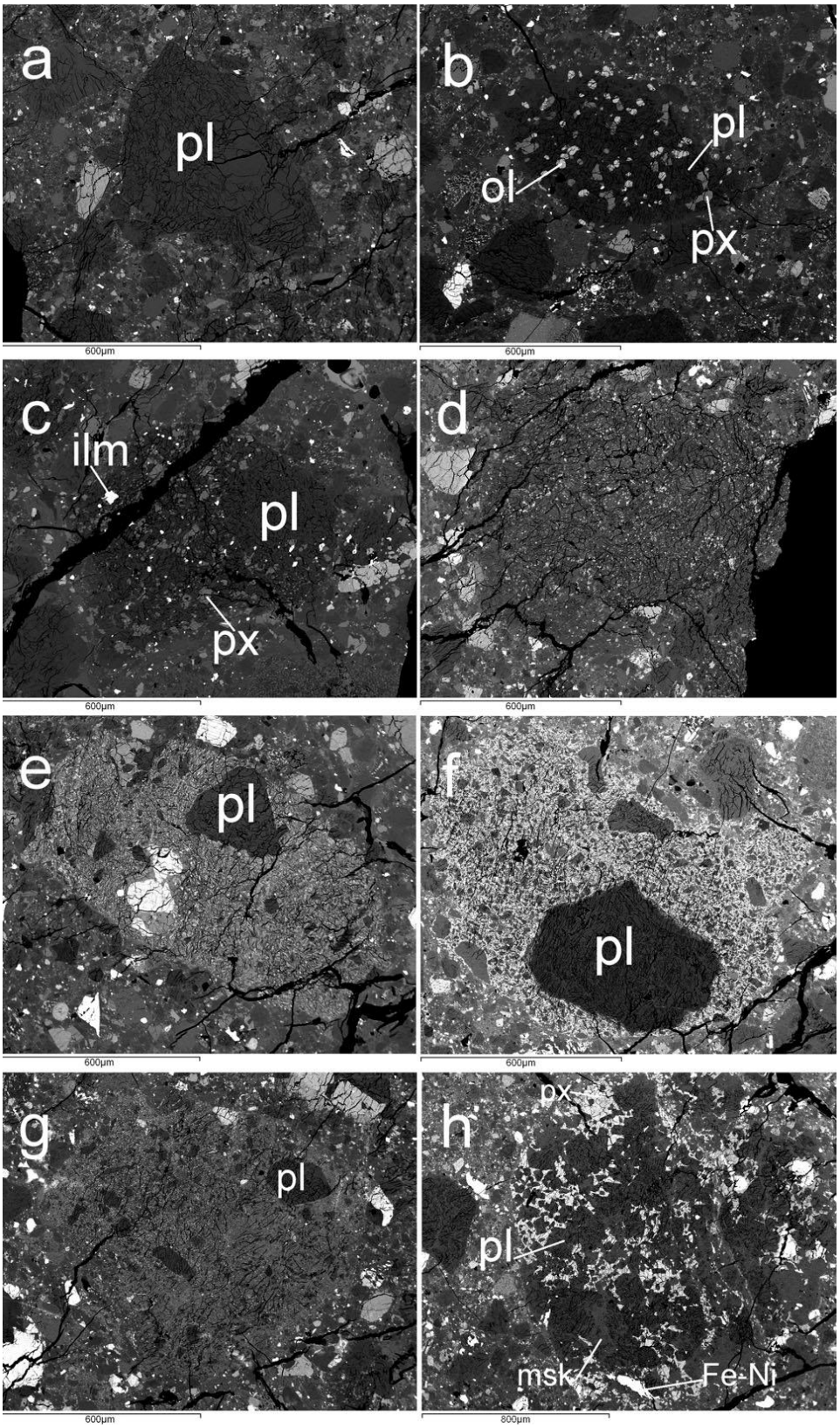

***Figure 8**: Backscattered electron images of 8 clasts in MIL 090036 ,34 (figure from Calzada-Diaz et al. 2016).*

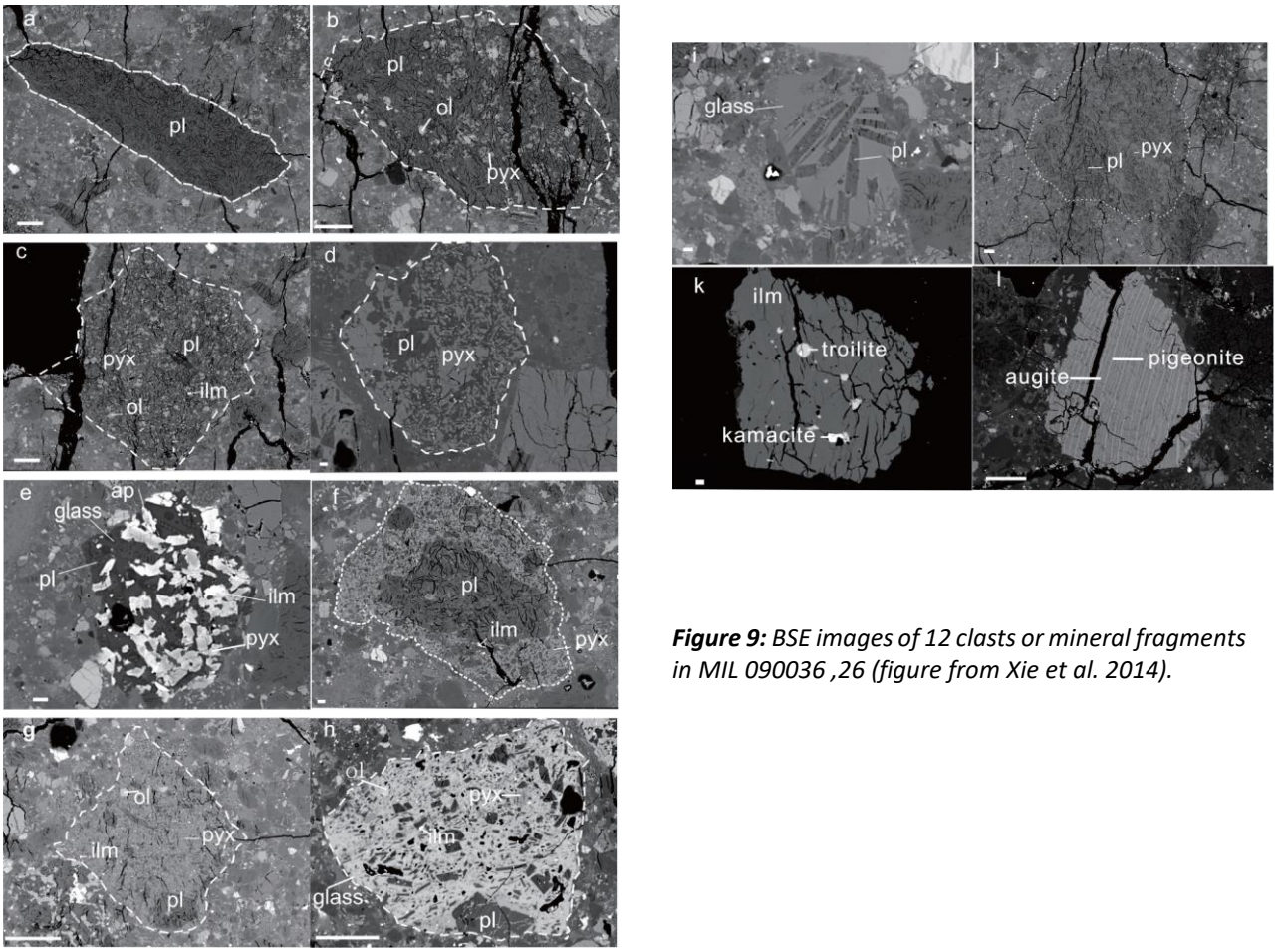

Figure 9: *BSE images of 12 clasts or mineral fragments in MIL 090036 ,26 (figure from Xie et al. 2014).*

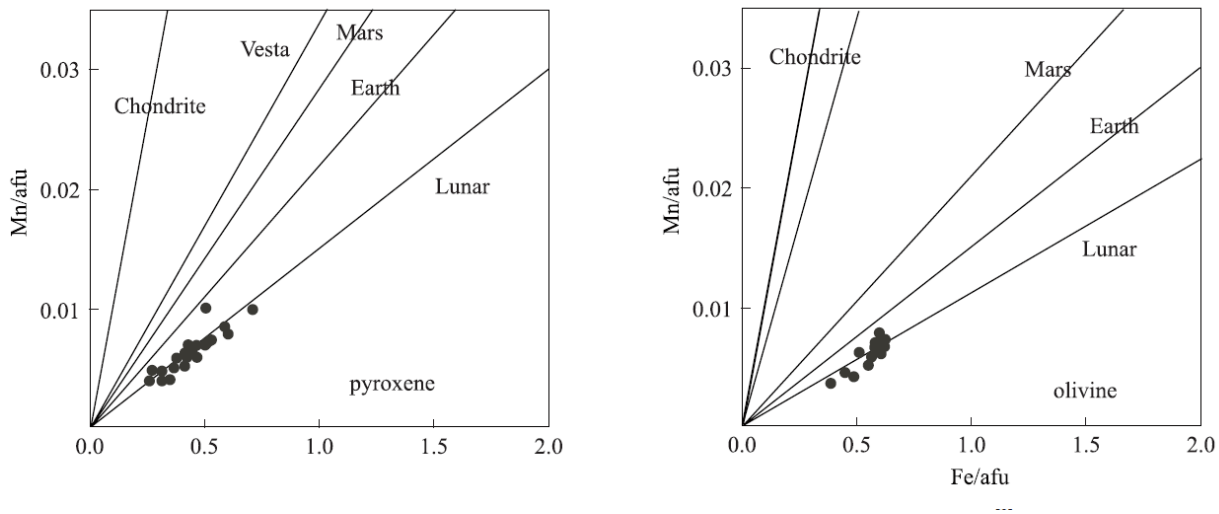

Figure 10*: Fe/Mn versus Fe (atomic formula unit) for pyroxene (left) and olivine (right) from lithic materials and mineral clasts from MIL 090036 (from Xie et al. 2014).*

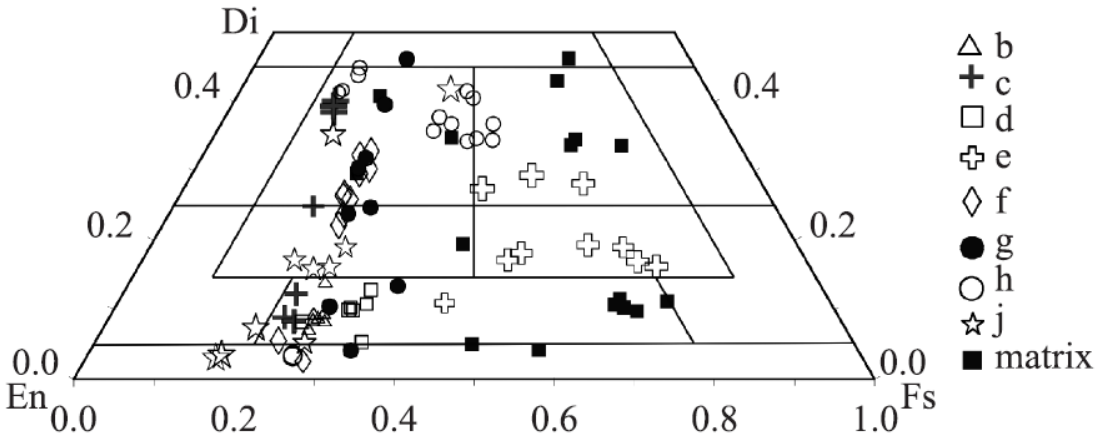

Figure 11*: Pyroxene quadrilateral showing compositions of pyroxenes in clasts b through J and matrix (figure from Xie et al., 2014).*

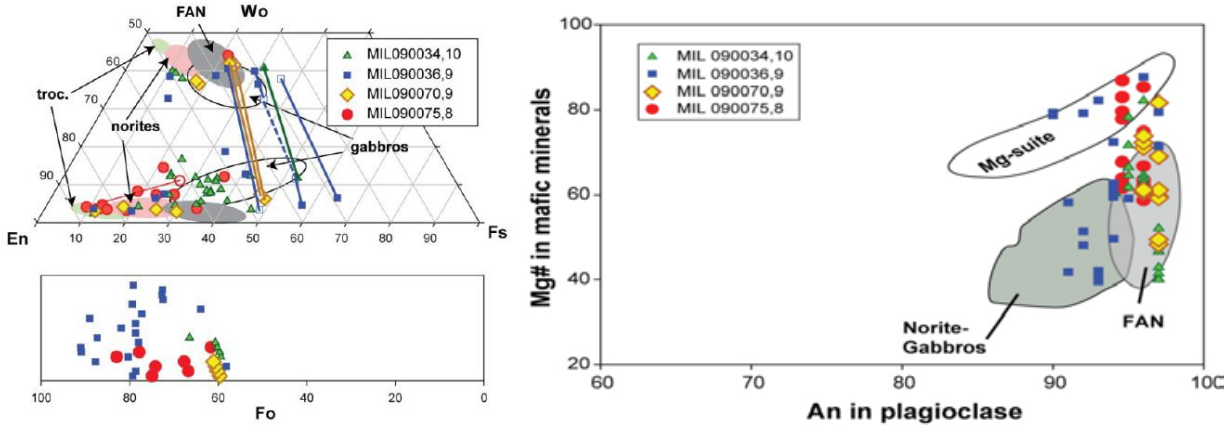

Figure 12: *Pyroxene and olivine mineral composition data for clasts and matrix in MIL 090036; pyroxene is more Fe-rich than other MIL09 anorthositic breccias while the olivine is more Mg-rich (left). Mg# (atomic Mg/(Fe + Mg) x 100) versus An in plagioclase showing the distinct compositions of MIL 090036 compared to the other MIL 09 breccias (figures from Liu et al., 2011).*

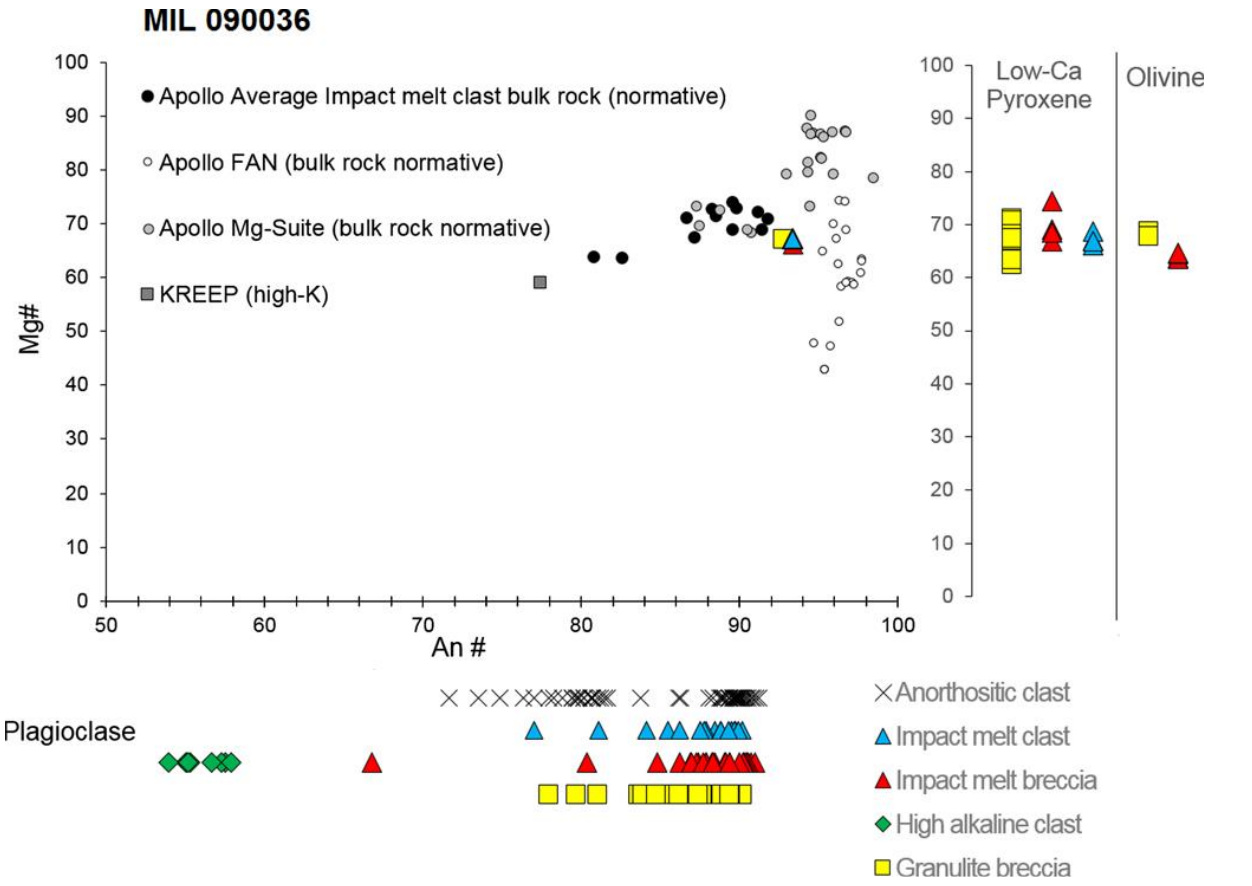

Figure 13: *Mg# of mafic minerals versus An content of plagioclase for clasts in MIL 090036 (top) and compositions of plagioclase grains in MIL 090036 (bottom) (figures from Calzada-Diaz et al. 2016).*

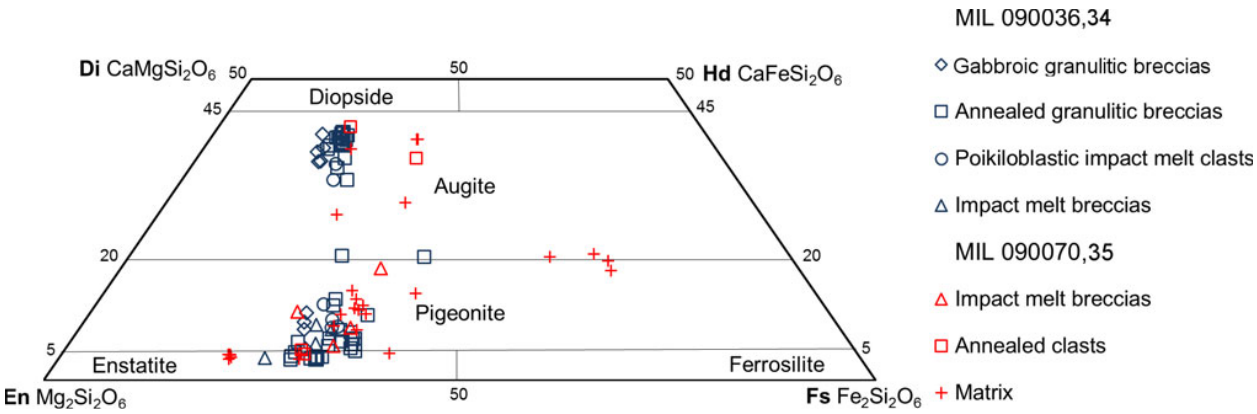

Figure 14: *Pyroxene quadrilateral showing compositions of pyroxenes in various clasts in MIL 090036 compared to MIL 090070 (figures from Calzada-Diaz et al. 2016).*

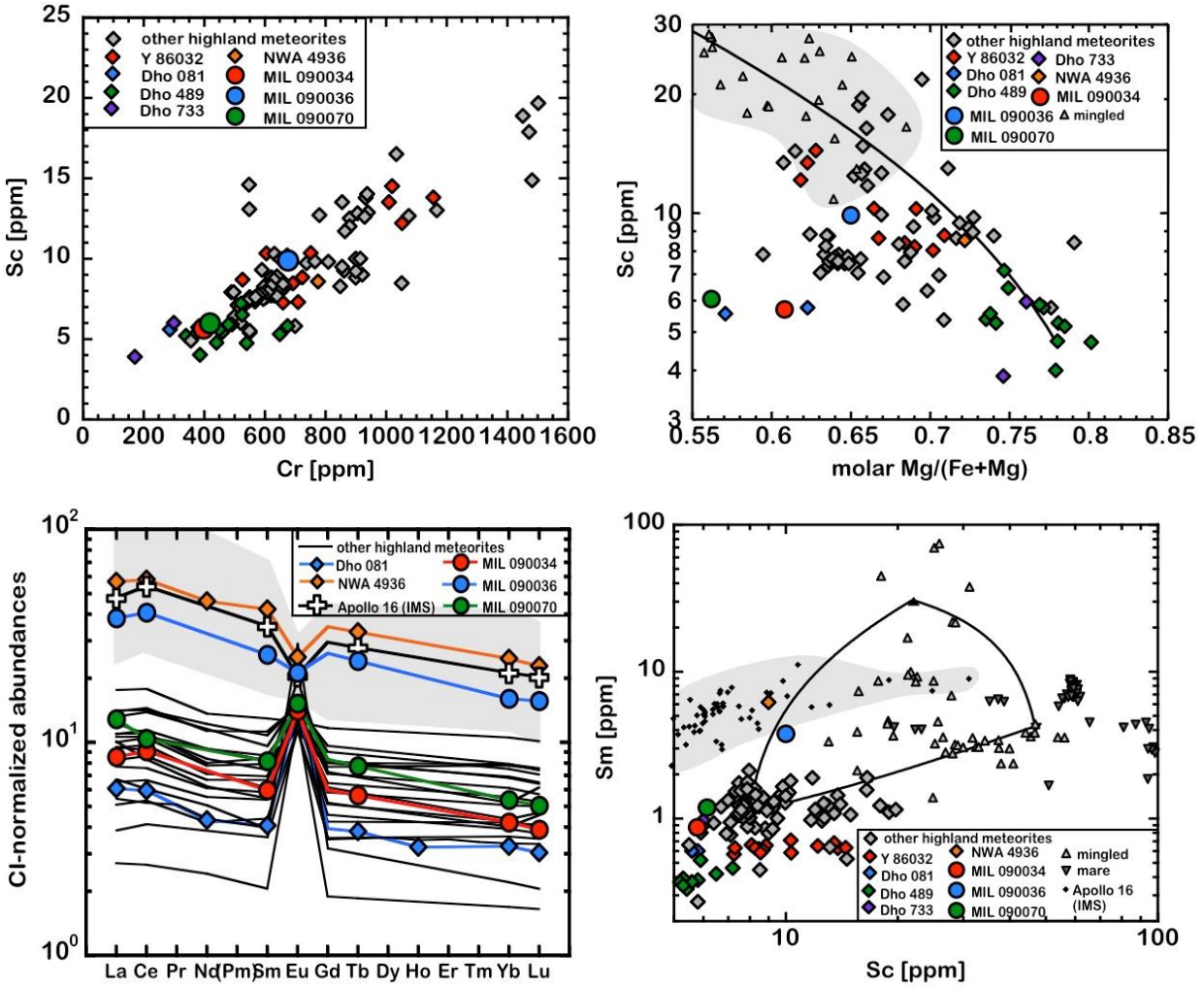

Figure 15*: Upper left: Cr vs. Sc abundances for lunar highland meteorites; upper right: Mg number vs. Sc abundances for lunar highland meteorites. Line represents mixing line of lunar highland meteorites (Dho 489 from Takeda et al., 2006) and mare basalt (Y 793169 from Warren and Kallemeyn, 1993); lower left: CI-normalized rare earth elements abundances for lunar highland meteorites and impact melt splashes from Apollo 16. Light dark shaded regions represent compositional ranges of impact melt splashes from Apollo 16 (Morris et al., 1986); lower right: Sc vs. Sm abundances for lunar highland, mingled and mare meteorites. Lines represent mixing line of FHT, PKT and maria. Data of FHT, PKT and maria, and impact melt splashes from Apollo 16 are taken from Korotev et al. (2009) and Morris et al. (1986) (figures from Shirai et al. 2012).*

Chemistry

MIL 090036 is compositionally distinct from the other MIL 09 lunar breccias. In particular it has slightly higher FeO and incompatible element concentrations such as Na_2O, Sm, Sc, La, and Yb, but lower Al_2O_3 (**Figure 15-17**). In addition, Cr is higher as well as Mg# (Figure 15,16), and MIL 090036 has a small negative Eu anomaly compared to the positive anomalies measured in the other MIL 09 lunar breccias (**Fig. 15**). These traits all suggest the minor presence of a KREEP component in MIL 090036, that distinguishes it compositionally from the other MIL 09 lunar breccias (Calzada-Diaz et al., 2016, Xie et al., 2014, Zeigler et al., 2016, Shirai et al., 2012, Liu et al., 2011, Korotev and Ziegler, 2015).

MIL 090036 has been included in a few focused isotopic studies. Ne and Xe isotopes indicate that there is a dominant cosmogenic component in MIL 090036 compared to other MIL 09 lunar breccias (**Figure 18**; Park et al., 2019). The potassium isotopic composition of MIL 090036 falls within the range of lunar samples in general, but again is distinct from the other MIL 09 lunar breccias (Tian et al., 2020). Finally, the MIL 090036 Os isotopic and HSE concentrations were analyzed as part of a broader study to examine the composition of impactors striking the Moon over time and various locations (McIntosh et al., 2020).

Radiogenic age dating and cosmogenic exposure ages

Reported $^{39}Ar/^{40}Ar$ ages (summarized in **Fig. 19-20**) suggest that the last major argon isotope resetting event in MIL 090036 took place at ~3.54 Ga (Park et al. 2013; Nyquist et al. 2016). MIL 090036 has a cosmic ray exposure of ~50±10 Ma (Nishiizumi and Caffee 2013). ^{37}Ar analyses indicate >103 Ma exposure age (Park et al. 2013; **Figure 21**). Both of these ages are higher than the other MIL 09 lunar breccias, and suggest an origin from shallow subsurface (depths ~100 cm). Altogether MIL 090036 likely had a short transit time, arriving on the Earth as a meteorite 0.1–0.2 Ma ago (Calzada-Diaz et al., 2016; Nishiizumi and Caffee, 2013).

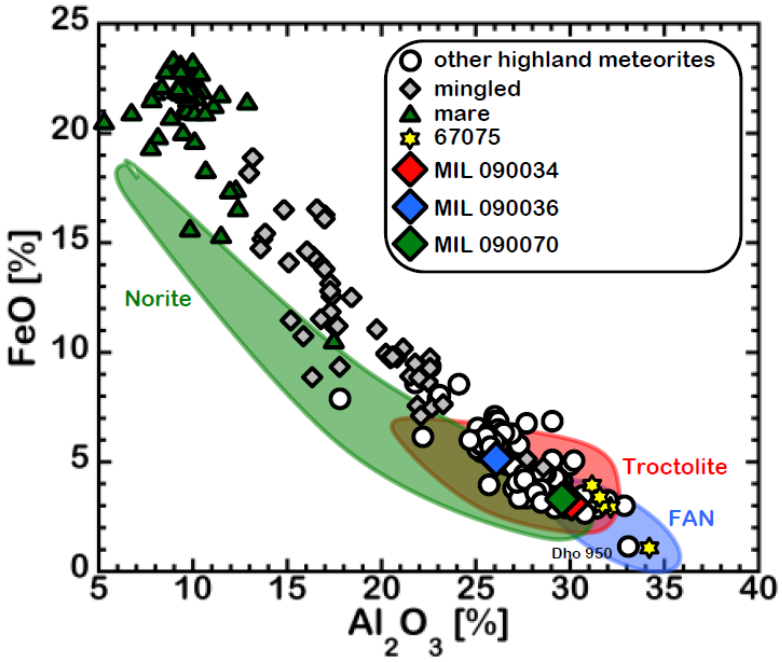

Figure 16: *Although all of the MIL 09 lunar breccias plot within the troctolite field, only MIL 090034 and MIL 090070 fall within the FAN field, this showing the distinctly different composition of MIL 090036 (from Park et al. 2013).*

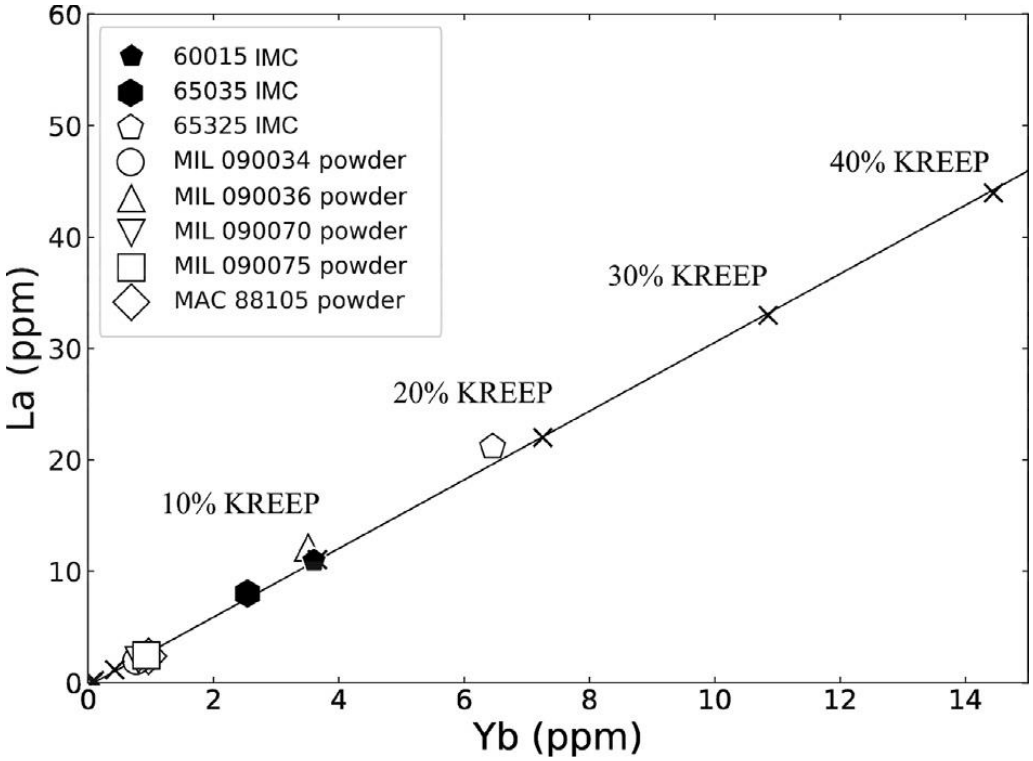

Figure 17: *Demonstration of slightly larger KREEP component present in MIL 090036 (open triangle) and similar to Apollo 16 impact melt clasts, compared to the other MIL 09 lunar breccias, based on La and Yb contents (from McIntosh et al., 2020).*

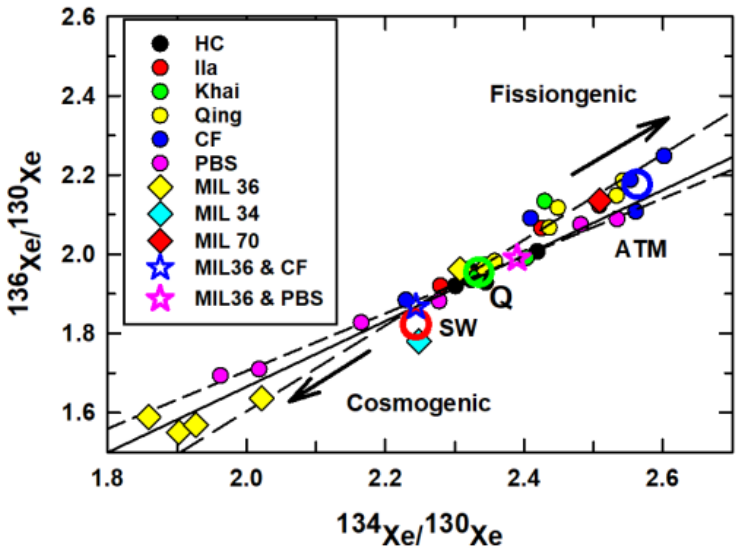

Figure 18*: $^{136}Xe/^{130}Xe$ vs. $^{134}Xe/^{130}Xe$ for lunar and enstatite meteorites near Solar Wind (SW), Q, and terrestrial atmosphere compositions (ATM). HC = Happy Canyon, Ila = Ilafegh, Khai = Khairpur, Qing = Qingzhen, CF = Cumberland Falls, PBS = Peña Blanca Springs. The most cosmogenic data for MIL 090036 and most fissionogenic data for CF are not shown. Intersections for regression lines are shown by open stars color-coded to the corresponding data, trapped compositions by open circles (figure from Park et al., 2019).*

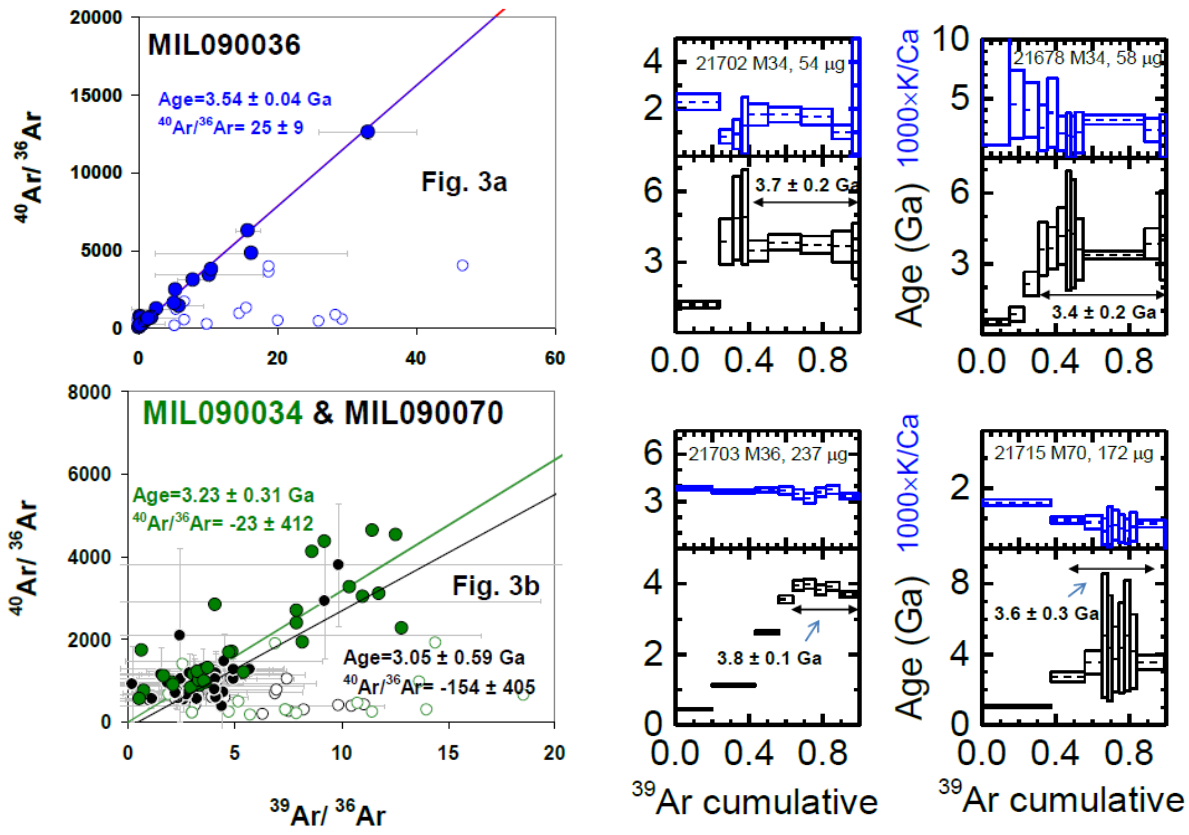

Figure 19: ***left:*** *$^{40}Ar/^{36}Ar$ vs. $^{39}Ar/^{36}Ar$ isochrons for MIL 090036 (a) and MIL 090034 plus MIL 090070 (b). Low temperature data shown by open symbols were excluded from the regressions.* ***Right:*** *Apparent Age spectra and K/Ca ratios of MIL 090034, MIL 090036 and MIL 090070 (figures from Park et al. 2013).*

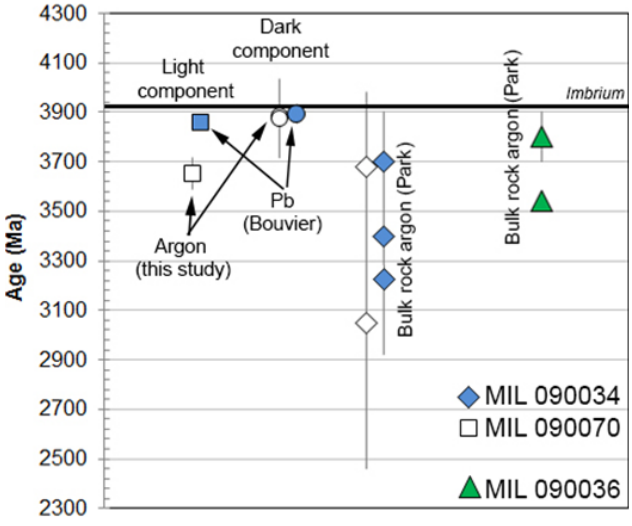

Figure 20: *Summary of events recorded by Ar and Pb isotopes for components and bulk-rock samples of MIL 090034 (Bouvier et al. 2013; Park et al. 2013), MIL 090070 (Park et al. 2013; Bouvier et al. 2013; and Calzada-Diaz et al. 2016). Park et al. (2013) determined argon isotope plateau and normal isochron age models. Bouvier et al. (2013) report Pb isotopes. The data from Calzada-Diaz et al. 2016 reflect argon fusion ages and a plateau age. Age of the Imbrium basin-forming event is shown for reference using the reported age of Snape et al. (2015) of 3915 Ma (figure from Calzada-Diaz et al. 2016).*

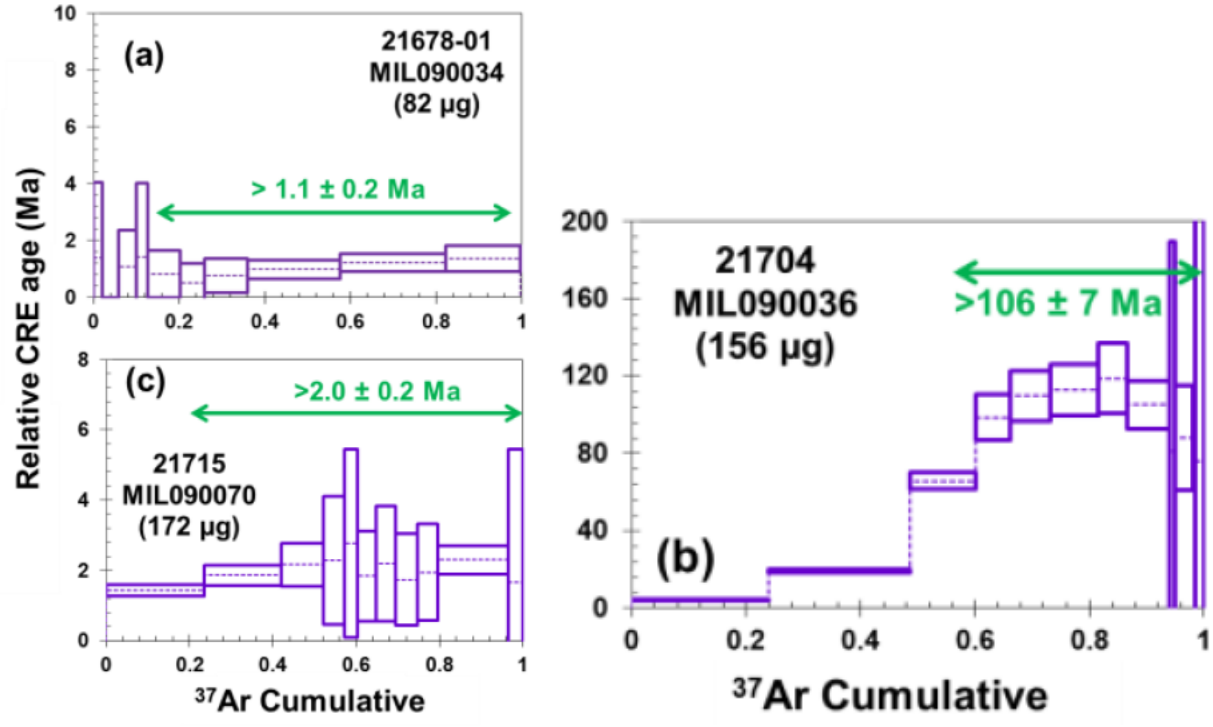

Figure 21: *Lower bounds on the relative CRE ages (values above arrows) differentiate MIL 090034, and MIL 090070 from MIL 090036 (figures from Park et al. 2013).*

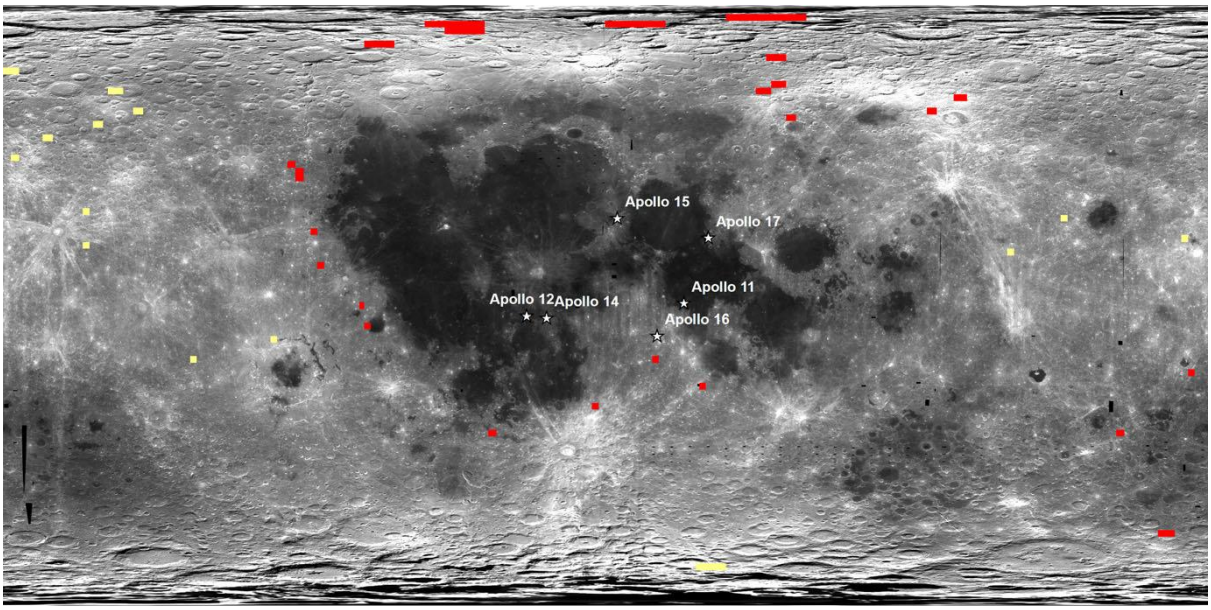

Figure 22*: Image showing the areas where surface regolith FeO, TiO_2, and Th composition measurements obtained by Lunar Prospector Gamma Ray Spectrometer (Prettyman et al. 2006) match the analytical composition of regolith breccias MIL 090036 in red and MIL 090070 and paired stones MIL 090034 and MIL 090075 (Korotev and Zeigler 2015) in yellow. Underlying albedo image of the Moon is a Clementine albedo map in a cylindrical projection with 0° longitude in the center (from Calzada-Diaz et al. 2016).*

Splits of MIL 090036 as of January 2024 (not including attrition)

split	parent	form	PI-1	PI-2	current	
0	-	DOC PC	-	-	JSC	
1	0	PB	-	-	JSC	
2		CPS+FI	-	-	JSC	
4	1	TS	SI		SI	
5	1	TS	Treiman	-	Treiman	
6	1	TS	Korotev	-	JSC	
7	1	THK	Liu	-	Liu	
8	1	TS	Liu	-	JSC	
9	1	TS	Liu	-	Liu	
11		CPS	Korotev	-	JSC	
12		EX CPS	Nishiizumi	-	Nishiizumi	
13		IN CPS	Nishiizumi	-	Nishiizumi	
14		CPS	Liu	-	Liu	
15		CPS	Korotev	-	JSC	
16		CPS	Yamaguchi	-	Yamaguchi	
17	0	PB	-	-	JSC	
18		CPS	Korotev	-	JSC	
19		DOC CP	Britt	-	JSC	
20		IN CPS	-	-	JSC	
21		CPS+FI	-	-	JSC	
23	17	TS	Yamaguchi	-	Yamaguchi	
24	17	THK	Joy	-	JSC	
25	17	TS	Joy	-	JSC	
26	17	TS	Miao	-	JSC	
27	21	PB	-	-	JSC	
29	27	TS	Zeigler	-	Zeigler	
30		IN CP	Joy	Curran	Curran	
32		IN CP	Crawford	-	consumed	
34	27	THK	Crawford	-	Crawford	
35		DOC PC	Evans	-	JSC	CT scanned
36		DOC PC	-	-	JSC	
37		CPS+FI	-	-	JSC	
39		INT CP	Wang	-	consumed	
43	21	polished CP	Madariaga	-	Madariaga	
45	27	TS	Gross	-	Gross	
47	35	DOC CP	-	-	JSC	
48	35	INT CP	Kruijer	-	Kruijer	
49	35	INT CP	Sehlke	-	Sehlke	
50	35		-	-	JSC	

Summary

Studies of the mineralogy, petrology, and geochemistry of MIL 090036 have shown that it is a mixture of different feldspathic lithologies including granulitic breccias, impact melt breccias, and plagioclase and pyroxene mineral clasts and fragments. MIL 090036 is compositionally and isotopically distinct from other MIL 09 lunar breccias. It has a minor KREEP component and is compositionally similar to Apollo 16 materials. Comparison of bulk FeO, TiO_2, and Th in MIL 090036 to global lunar geochemical data shows a potential origin in the surroundings outskirts of the Procellarum KREEP Terrane (**Fig. 22**).

References:

Calzada-Diaz, A., Joy, K. H., Crawford, I. A., & Strekopytov, S. (2017) The petrology, geochemistry, and age of lunar regolith breccias Miller Range 090036 and 090070: Insights into the crustal history of the Moon. . Meteoritics & Planetary Science, 52, 3-23, doi: 10.1111/maps.12737.

Curran, N.M., Joy, K.H., Snape, J.F., Pernet-Fisher, J.F., Gilmour, J.D., Nemchin, A.A., Whitehouse, M.J., and Burgess, R. (2019) The early geological history of the Moon inferred from ancient lunar meteorite Miller Range 13317. *Meteoritics & Planetary Science*, 54, 1401-1430, doi: 10.1111/maps.13295.

Korotev, R.L., and Zeigler, R.A. (2015) ANSMET Meteorites from the Moon. In Righter, K., Corrigan, C.M., McCoy, T.J., and Harvey, R.P. *Meteorites: A Pictorial Guide to the Collection*, First Edition, AGU Wiley, pp. 101-130.

Liu, Y., Patchen, A., & Taylor, L. A. (2011) Lunar highland breccias MIL 090034/36/70/75: A significant KREEP component. In *42nd Annual Lunar and Planetary Science Conference* (No. 1608, p. 1261).

McIntosh, E. C., Day, J. M. D., Lui, Y., Jiskoot, C. (2020) Examining the compositions of impactors striking the Moon using Apollo impact melt coats and anorthositic regolith breccia meteorites. Geochimica et Cosmochimica Acta, 274, 192-210, doi: 10.1016/j.gca.2020.01.051.

Nishiizumi, K., & Caffee, M. W. (2013) Relationships among six lunar meteorites from Miller Range, Antarctica based on cosmogenic radionuclides. In *44th Annual Lunar and Planetary Science Conference* (No. 1719, p. 2715).

Park, J., Nyquist, L. E., Shih, C. Y., Herzog, G. F., Yamaguchi, A., Shirai, N., ... & Swisher, C. C. (2013) Late Bombardment of the Lunar Highlands Recordeded in MIL 090034, MIL 090036 and MIL 090070 Lunar Meteorites. In *44th Annual Lunar and Planetary Science Conference* (No. 1719, p. 2576).

Park, J., Nagao, K., Nyquist, L.E., Herzog, G.F., Choi, J., Baek, J.M., Park, C., Lee, J.I., Lee, M.J., Weisberg, M.K. and Ebel, D.S. (2019) Noble Gas Studies of Lunar and Enstatite Meteorites. In *50th Annual Lunar and Planetary Science Conference* (No. 2132, p. 2272).

Satterwhite, C. E. and Righter, K. (2010) Ant. Met. Newsl. 33 no. 2.

Shirai, N., Ebihara, M., Sekimoto, S., Yamaguchi, A., Nyquist, L., Shih, C.Y., Park, J. and Nagao, K. (2012) Geochemistry of Lunar Highland Meteorites MIL 090034, 090036 and 090070. In *43rd Annual Lunar and Planetary Science Conference* (No. 1659, p. 2003).

Tian, Z., Jolliff, B.L., Korotev, R.L., Fegley, B., Lodders, K., Day, J.M.D., Chen, H., Wang, K. (2020) Potassium isotopic composition of the moon. Geochimica et Cosmochimica Acta, 280, 263-280, doi: 10.1016/j.gca.2020.04.021.

Xie, L., Chen, H., Miao, B., Xia, Z., and Yao, J. (2014) Petrography and mineralogy of new lunar meteorite MIL090036. *Advances in Polar Science 25*, 17-25.

Zeigler, R. A., & Korotev, R. L. (2016) Petrography and Geochemistry of Lunar Meteorite Miller Range 13317. In *47th Annual Lunar and Planetary Science Conference* (No. 1903, p. 2554).

Kevin Righter, April 2024